

Multiphoton Amplification and Squeezing by a Nonlinear Nanomechanical Mode

J. S. Ochs,^{1,*} M. Seitner,¹ M. I. Dykman,² and E. M. Weig¹

¹*Department of Physics, University of Konstanz, 78457 Konstanz, Germany*

²*Michigan State University, East Lansing, MI 48824, USA*

(Dated: October 25, 2021)

Because of their small decay rates, nanomechanical modes enable studying strongly nonlinear phenomena already for a moderately strong resonant driving. In particular, the response to an additional weak probe field becomes multiphoton, in quantum terms. Here we experimentally demonstrate resonant multiphoton amplification and resonant absorption of the probe field. The corresponding spectral peaks lie on the opposite sides of the strong-drive frequency and are separated from it by the frequency of the weakly damped vibrations about the stable state of the strong-drive-induced oscillations. Even though the system is far from equilibrium and the fluctuation-dissipation theorem does not apply, we show that the response to the probe field allows us to characterize the squeezing of fluctuations about the stable states of forced oscillations. Our two-tone experiment is done in the classical regime, but our findings should equally apply to quantum fluctuations as well. The squeezing parameter extracted from the spectra of the response is in excellent agreement with the calculated value with no free parameters.

I. INTRODUCTION

Nanomechanical vibrational systems have been traditionally studied in the context of mesoscopic condensed matter physics and nonlinear dynamics, and more recently also from the perspective of quantum and classical nonlinear optics [1–3] and quantum information [4–6]. Different nanomechanical vibrational modes are strongly localized within the resonator, they are well separated in frequency and well-characterized. They often have a very high quality factor Q , which is determined by the ratio of the vibration frequency to the decay rate and can exceed 10^8 [7, 8]. The modes can be easily driven into a nonlinear regime, and a host of nonlinear phenomena has been explored, from vibration bistability and associated effects, cf. [9–16], to nonlinear mode coupling, frequency mixing, chaos, and a frequency comb generation, cf. [17–25], and to processes that involve spontaneous or stimulated Raman scattering and are largely exploited in the context of cavity optomechanics [26].

An important group of applications of nanomechanical systems is related to the mass, charge, and force sensing. A fundamental constraint on the sensitivity of the measurements is imposed by noise. The noise comes from classical sources as well as from quantum fluctuations. A well-established by now approach to suppressing quantum noise is based on using squeezed states [27]. It has been recently implemented in laser interferometers for gravitational wave detection [28, 29]. With the techniques of the cavity optomechanics, squeezing in the quantum regime has been also achieved in mechanical systems [30–32]. In quantum squeezing, the variance of one of the quadratures of the vibrations is reduced below its value in the ground vibrational state, whereas fluctuations of the other quadrature are increased. This

is a consequence of the uncertainty principle, since the quadrature operators correspond to the scaled vibration coordinate and momentum in the rotating frame and do not commute.

However, squeezing is not limited to the quantum domain. One may expect squeezing to occur for classical fluctuations, too, in which case fluctuations of one of the quadratures are smaller than in thermal equilibrium. For a degenerate parametric mechanical amplifier, squeezing of classical fluctuations was first demonstrated by Rugar and Grütter [33].

Squeezing should generically emerge in periodically driven vibrational systems. This is a consequence of the broken continuous time-translation symmetry. The continuous symmetry leads to equal variances of the quadrature fluctuations, since the quadratures can be interchanged by shifting the time by a quarter of the vibration period. A periodic driving makes such shifting impossible. Therefore, along with the traditionally explored squeezing due to parametric driving [34], squeezing should result from driving a nonlinear vibrational mode close to its eigenfrequency, and the effect may be resonantly strong. The occurrence of squeezing in this case could be inferred already from the early work on resonantly driven nonlinear modes [35, 36]. A theory of squeezing was developed by Buks and Yurke [37], and the effect was first observed in a nanomechanical Duffing resonator by Almog et al. [38]. This observation was based on the conventional homodyne detection scheme and was done in a narrow parameter range near the cusp on the bifurcation curve.

Homodyne measurements are strongly impeded by frequency fluctuations, which play an important role in nanomechanical systems. The limitations are particularly strong in systems with small damping, where the uncertainty in the in-phase component due to slow frequency fluctuations becomes large [39]. No homodyne measurements of squeezing have been reported for strongly underdamped vibrational systems, to the best

* née Huber

of our knowledge. However, it was demonstrated [40], that the squeezing of classical fluctuations in strongly underdamped resonantly driven systems can be found by measuring their power spectrum. The power spectrum is asymmetric. The asymmetry comes along with the squeezing [41] as a consequence of a resonant driving, which allows one to find the squeezing parameter in the classical regime.

In this paper we demonstrate that the squeezing parameter of a strongly driven underdamped nanomechanical system can also be determined by measuring the spectrum of the response of the system to an additional weak probe force. A major advantageous feature of this result is that, although the experiment is carried out where the dynamics of the system is classical, the method is not limited to the classical regime. It can be equally well applied to characterize squeezing of quantum fluctuations in a strong resonant field, since the features of the response to a weak field are temperature-independent.

For weak damping the absorption spectrum of the probe field should display two peaks, where the mode has one stable state of forced vibrations (and up to five peaks where there are two stable vibrational states) [35, 41, 42]. Expanding on the previous results, we show that the difference between the two peaks is determined by the squeezing parameter, which is similar to the case of the power spectrum in the classical regime [40]. We note that the onset of the two peaks induced by a probe force in the vibration amplitude of a mechanical mode was seen by Antoni *et al.* [43], but the question of squeezing was not addressed in this paper.

Besides the squeezing, we wish to highlight another aspect of the response of the resonantly driven system to a probe force. One of the two peaks corresponds to an amplification of this force. Such amplification can be thought of in terms of parametric amplification in nonlinear optics [44]. However, the process is more complicated. In optics terms, it is a multiphoton process, as we explain in Sec. IV. We report a direct observation of this effect.

Below in Section II we describe the setup of the experiment and in Section III describe the experimental observations. In Section IV we introduce the squeezing parameter and give explicit expressions of the susceptibility in terms of this parameter. Section V we describes the results of the measurements of the squeezing parameter and its dependence on the driving force. Section VI contains concluding results.

II. SETUP AND CHARACTERIZATION

The nanomechanical resonator under investigation is a doubly clamped, strongly pre-stressed silicon nitride string resonator fabricated on a fused silica substrate, similar to the one depicted in Fig.1(a) and described in reference [40]. It is 270 nm wide, 100 nm thick and 55 μm long. The string resonator (green) is flanked by

two adjacent gold electrodes (yellow), enabling the dielectric transduction combined with a microwave cavity-enhanced heterodyne detection scheme discussed in [45–47]. A schematic circuitry of the setup is displayed in the inset of Fig.1(a). The microwave cavity is pumped on resonance at ≈ 3.6 GHz to facilitate displacement detection while avoiding unwanted dynamical backaction effects. Actuation and eigenfrequency tuning of the string is accomplished by applying a dc voltage along with a near-resonant rf drive voltage $V_d \cos(\omega_d t)$. A weak probe tone $V_p \cos(\omega_p t)$ is additionally scanned across the resonance to record the response spectrum of the device within a small frequency span. The two-tone measurements are performed using a fast lock-in amplifier (LA) with a multi-frequency option. For all measurements presented in the following, a constant dc voltage of 5 V is applied such that the fundamental flexural out-of-plane mode can be considered independently, avoiding a hybridization with the in-plane mode [48]. The experiment is performed at room temperature of 293 K and under vacuum at a pressure of $\leq 10^{-4}$ mbar.

The displacement $q(t)$ of the single mode can be described by the following equation of motion

$$\ddot{q} + 2\Gamma\dot{q} + \omega_0^2 q + \gamma q^3 = F_d \cos(\omega_d t) + F_p \cos(\omega_p t) + \xi(t). \quad (1)$$

Here, $\omega_0 = 2\pi f_0$ is the angular eigenfrequency, Γ the damping rate and γ the Duffing nonlinearity parameter. A comparatively strong driving force with amplitude F_d and frequency $\omega_d = 2\pi f_d$ is applied; in this experiment, we use a resonant drive and set $\omega_d = \omega_0$. The additionally applied weaker force probing the response of the device in the vicinity of the resonance has amplitude F_p and frequency $\omega_p = 2\pi f_p$. The third force term $\xi(t)$ represents the thermal noise. The effective mass of the resonator is, for the time being, is set to $m = 1$. As both the drive tones and the measured signal are voltage signals, we calibrate the system in units of volts, as discussed in detail in the Sup. Mat. of Ref. [40].

In the absence of the weak probe tone ($V_p = 0$) and using a small amplitude of the drive V_d we sweep the frequency ω_d to study the linear response of the fundamental out-of-plane mode at an eigenfrequency of $f_0 = 6.528$ MHz. It is shown for a drive of $V_d = 1$ mV as a function of the detuning $f_d - f_0$ in Fig.1(b) as black dots. A Lorentzian fit (red solid line) yields a linewidth $2\Gamma/2\pi = 20$ Hz and a quality factor of $Q \approx 325,000$.

Increasing the drive voltage leads to the well-known Duffing response. A bidirectional response curve at a drive voltage of $V_d = 20$ mV is plotted in Fig.1(c) as black dots. A fit with the Duffing model (red line) allows to extract the Duffing nonlinear parameter $\gamma/(2\pi)^2 = 2.8 \cdot 10^{15} \text{ V}^{-2} \text{ s}^{-2}$.

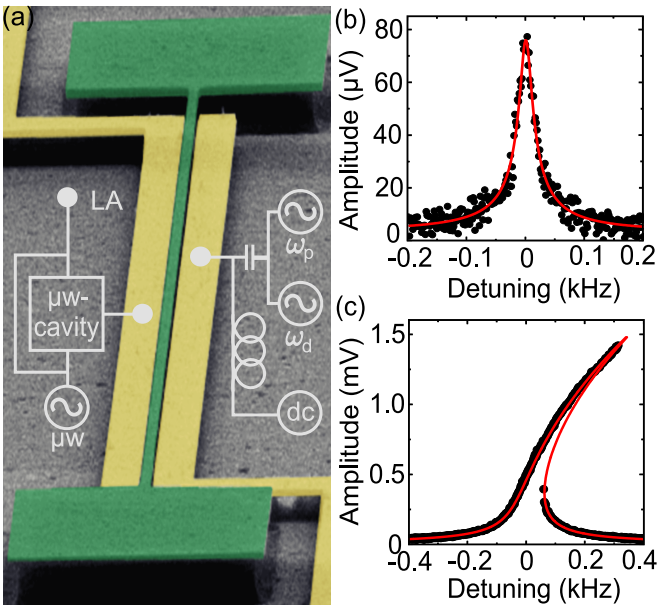


Figure 1. (a) Scanning electron micrograph of the doubly clamped silicon nitride sting resonator (green) and two adjacent gold electrodes (yellow) for dielectric drive and detection. Inset displays a schematic of the experimental setup. (b) Linear response of the fundamental flexural out-of-plane mode at a drive voltage of $V_d = 1$ mV (black dots). A Lorentzian fit (red) yields an eigenfrequency of 6.528 MHz, a linewidth of $2\Gamma/2\pi = 20$ Hz and a quality factor of $\approx 325,000$. (c) Duffing response at a drive voltage of $V_d = 20$ mV (black dots) and fit with the Duffing model (red). The resulting Duffing nonlinearity is $\gamma/(2\pi)^2 = 2.8 \cdot 10^{15} \text{ V}^{-2} \text{ s}^{-2}$.

III. EXPERIMENTAL OBSERVATIONS

The measurements described in the following are performed using the two-tone scheme introduced in Fig. 1(a). The resonant drive tone applied at $f_d = f_0$ is increased from 0 to 100 mV. As the drive is applied on resonance, the nonlinear resonator exhibits only one stable state (cf. Fig. 1(c)). The weak probe tone with amplitude V_p is swept across the resonance with a bandwidth of 5 Hz and an 8th order filter of the fast lock-in amplifier. We record the in-phase and quadrature components of the vibrations at the probe frequency. We verified that the amplitude of these vibrations was proportional to V_p in the studied range of V_p , indicating that the results refer to the regime of the linear response to the probe force. Figure 2(a) displays the spectra of this response to a probe of $V_p = 3$ mV for different amplitudes of the strong force using a color-coded amplitude.

Two distinct peaks, equally spaced from the line at the frequency of the strong drive (i.e., $f_p - f_d = 0$) and with a power-dependent splitting are observed. As will be shown in Sec. IV, these two peaks originate from the probe-induced small-amplitude vibrations about the stable state of the vibrations induced by the strong drive. The bright horizontal line centered at the strong-drive

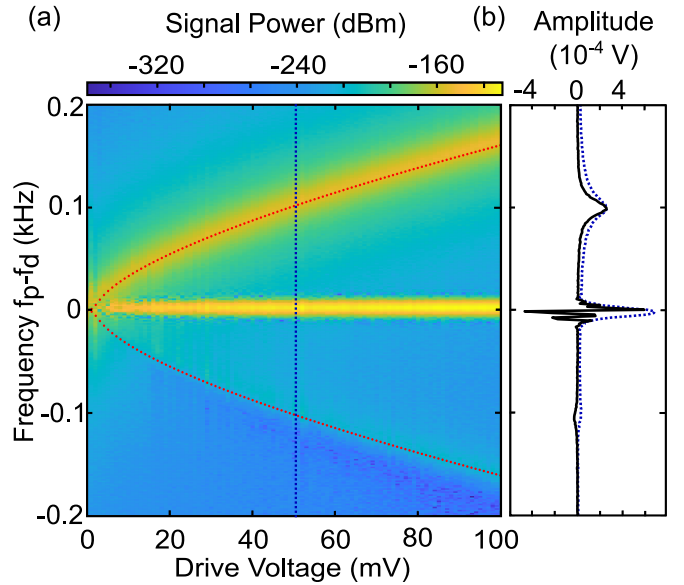


Figure 2. (a) Color-coded response spectra for increasing drive voltages at $f_p - f_d = f_0$. The probe tone is fixed to $V_p = 3$ mV. A central feature and two satellite peaks are clearly visible. The satellites have strongly different brightness. Their splitting increases with the increasing amplitude of the drive, in good agreement with the theoretical model of Eq. (3) which is plotted as red dots. The blue dotted line indicates the line cut discussed in panel (b). (b) Amplitude (blue dotted line) and quadrature component (black solid line) of the vibrations at the probe frequency for $V_d = 50$ mV.

frequency indicates the response of the resonator to the probe interfering with the strong drive tone.

The blue dotted line in Fig. 2 (a) indicates a single line scan of the response to the probe. It refers to a driving voltage of $V_d = 50$ mV. The amplitude of the vibrations at the probe frequency ω_p is shown as a blue dotted line in Fig. 2 (b). In addition, the quadrature component of these vibrations is plotted as a black solid line. These will be the signal components which will be discussed in more detail below. In both data sets the higher frequency satellite is much brighter than that at the lower frequency. As we will also discuss in the following, this is a spectral evidence of the thermomechanical squeezing induced by the strong drive, similar to what has been reported for the power spectrum [40]. In contrast to the amplitude data which features two positive satellites, the quadrature data exhibits different signs for the two satellites, a positive higher frequency, and a negative lower frequency satellite. Both satellites in the quadrature data have a Lorentzian line shape with the same linewidth $2\Gamma/2\pi = 20$ Hz, as the resonator. In contrast, the dependence of the amplitude on f_p is profoundly non-Lorentzian.

IV. SUSCEPTIBILITY OF A STRONGLY UNDERDAMPED, RESONANTLY DRIVEN MODE

Prior to analyzing the manifestation of squeezing in the response to the probe force, we consider the dynamics in the absence of the probe force and noise, i.e., for $F_p = 0$ and $\xi(t) = 0$ in Eq. (1). The driving in this case is sinusoidal. The stationary states of forced vibrations of a mode are formed on balance of the energy absorption from the driving force $F_d \cos \omega_d t$ and the energy drain to a thermal reservoir. However, if we think of the driving force as coming from an electromagnetic field (which is the case in the experiment), the absorption by a nonlinear mode is multiphoton. This is because the mode frequency depends on the amplitude, and thus, by changing the vibration amplitude, the field “prepares” the absorption coefficient. If the field is resonant, weakly damped modes display strong nonlinearity already for a comparatively weak force. The forced vibrations are essentially sinusoidal, but their amplitudes (and phases) can take two values, in a certain parameter range. These values $A_{1,2}$ are given, respectively, by the largest and smallest roots of the equation [49]

$$\begin{aligned} \varphi(3|\gamma|A_j^2/8\omega_d\Gamma) &= 0, \\ \varphi(\rho) &= \rho[(\rho - \Omega \operatorname{sgn}\gamma)^2 + 1] - \frac{3|\gamma|F_d^2}{32\omega_d^3\Gamma^3}, \quad \Omega = \frac{\omega_d - \omega_0}{\Gamma}. \end{aligned} \quad (2)$$

In what follows we assume $\gamma > 0$; this condition holds in our system. The occurrence of two stable values of A_j is seen in Fig. 1(c). The higher and lower branches of the amplitude A_j as function of ω_d in this figure correspond to $j = 1$ and $j = 2$, respectively.

For weak damping and weak nonlinearity it is convenient to describe the dynamics of the mode by switching to the rotating frame at the drive frequency ω_d . We introduce the scaled coordinate and momentum, Q and P , which correspond to the in-phase and the quadrature components of the vibrations,

$$q(t) + i\omega_d^{-1}p(t) = (Q + iP) \exp(-i\omega_d t), \quad [p(t) \equiv \dot{q}(t)]$$

[we note that the variables Q, P differ from the dimensionless variables Q, P in the previous work of one of us (MD), cf. [41], by a factor $(8\omega_d\Gamma\Omega/3\gamma)^{1/2}$]. The equations of motion for $Q(t), P(t)$ follow from Eq. (1). If we disregard small fast-oscillating corrections, i.e., use the rotating wave approximation (RWA) [50], the coefficients in these equations are independent of time, in the absence of noise and the weak probe $\propto F_p$. A j th stable state corresponds to a stable stationary solution (Q_j, P_j) of these equations, and $Q_j^2 + P_j^2 = A_j^2$.

The dynamics near a stable state is described by linearizing the equations of motion in $Q - Q_j, P - P_j$. In the weak-damping limit, the trajectories $Q(t) - Q_j, P(t) - P_j$ correspond to weakly decaying oscillations. The oscillation frequency is

$$\omega_j = \Gamma[(3\rho_j - \Omega)(\rho_j - \Omega)]^{1/2}, \quad \rho_j = \frac{3|\gamma|A_j^2}{8\omega_d\Gamma}. \quad (3)$$

The condition of the weak decay of the oscillations is $\omega_j \gg \Gamma$. We emphasize that ω_j is the oscillation frequency in the rotating frame, and therefore $\omega_j \ll \omega_0$. Therefore the inequality $\Gamma \ll \omega_j$ is a much stronger constraint on the decay rate Γ than the condition $\Gamma \ll \omega_0$ that the mode is underdamped. In our experiment the condition $\Gamma \ll \omega_j$ was satisfied. We note that, for small decay rate, $A_j^2 \approx Q_j^2$ and thus $\rho_j \approx 3|\gamma|Q_j^2/8\omega_d\Gamma$.

In the presence of a weak noise the driven mode mostly performs small-amplitude fluctuations about the stable state j it occupies. The power spectrum of these fluctuations has peaks at the frequencies $\omega_d \pm \omega_j$. Such well-resolved peaks were seen in our previous experiment [40]. The experiment was done in the classical regime, $k_B T \gg \hbar\omega_0$, and it was found that the areas of the peaks are different. Moreover, the area of one of the peaks was smaller than the area of the peak in the power spectrum at frequency ω_0 in the absence of the driving. This is a clear demonstration of the effect of squeezing of the fluctuations.

The squeezing is immediately seen in the expressions for the variances of the in-phase and quadrature components. With the account taken of both classical and quantum fluctuations [40, 41]

$$\begin{aligned} \langle \delta Q_j^2 \rangle &\equiv \langle (Q - Q_j)^2 \rangle = \frac{\hbar}{4\omega_d}(2\bar{n} + 1)(1 + e^{-4\phi_j}), \\ \langle \delta P_j^2 \rangle &\equiv \langle (P - P_j)^2 \rangle = \frac{\hbar}{4\omega_d}(2\bar{n} + 1)(1 + e^{4\phi_j}), \end{aligned} \quad (4)$$

where \bar{n} is the Planck number of the oscillator, $\bar{n} = [\exp(\hbar\omega_0/k_B T) - 1]^{-1}$. The squeezing parameter ϕ_j is given by the equation

$$\tanh \phi_j = \frac{|3\rho_j - \Omega|^{1/2} - |\rho_j - \Omega|^{1/2}}{|3\rho_j - \Omega|^{1/2} + |\rho_j - \Omega|^{1/2}}. \quad (5)$$

The sign of the parameter ϕ_j is determined by the sign of $\rho_j - \Omega$ (which coincides with the sign of $3\rho_j - \Omega$). One can see from Eqs. (2) and (3) that on the higher-amplitude branch in Fig. 1(c), i.e., for $j = 1$, we have $\phi_1 > 0$. For the lower branch, $j = 2$, the squeezing parameter is negative, $\phi_2 < 0$.

As seen from Eqs. (2) and (5), in the considered weak-damping limit, the squeezing parameter depends on a single combination of the parameters of the driven mode

$$\beta = 3\gamma F_d^2/[32\omega_d^3(\omega_d - \omega_0)^3] \quad (\gamma > 0). \quad (6)$$

As indicated in Eq. (6), the expression for β is written for the considered case $\gamma > 0$; an extension to the case $\gamma < 0$ is straightforward. The parameter ϕ as a function of β is shown in Fig. 3; in fact, we show directly the relevant parameter $\exp(4\phi)$. As seen from Fig. 3, ϕ monotonically

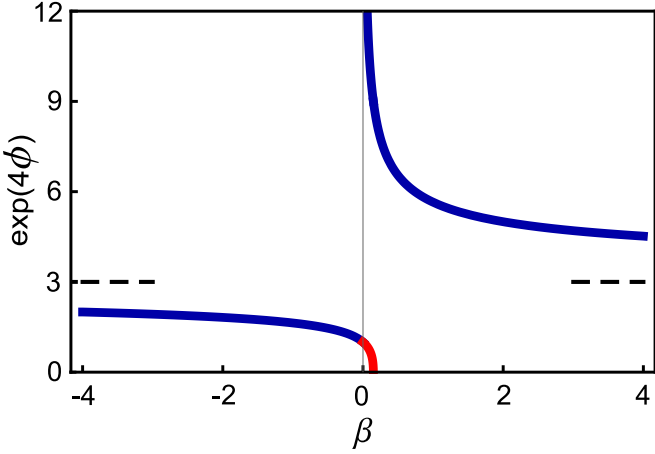


Figure 3. The dependence of the squeezing parameter on the parameter β , Eq. (6), in the limit of weak damping and for $\gamma > 0$. In this limit the bistability of forced vibrations, and thus the vibrational branch $j = 2$ exist in the range $0 < \beta < 4/27$. The red line shows $\exp(4\phi_2)$ in this range. The blue lines show $\exp(4\phi_1)$. Outside the bistability region the system has only one stable vibrational state, and $\phi_1 \equiv \phi$. The dashed lines show the limit of $\exp(4\phi_1)$ for $|\beta| \rightarrow \infty$ which, physically, corresponds to the driving frequency approaching the mode eigenfrequency, $|\omega_d - \omega_0| \rightarrow 0$. The weak-damping limit breaks down for small $\beta \rightarrow 0$ and, for the branch $j = 2$, for β approaching $4/27$.

decreases to zero as β increases from $-\infty$ to 0, and then ϕ decreases with the increasing β for $\beta > 0$. In the region $|\beta| \ll 1$ the approximation $\omega_j \gg \Gamma$ breaks down, which imposes a cutoff on $|\phi_{1,2}|$ for small $|\beta|$.

It follows from Eq. (4) that the variance of the in-phase component is below the standard limit $(\hbar/2\omega_0)(2\bar{n} + 1)$ for an undriven mode, which indicates the squeezing. At the same time, the product of the root-mean-square deviations $[(\langle (Q - Q_j)^2 \rangle \langle (P - P_j)^2 \rangle)]^{1/2} = (\hbar/2\omega_d)(2\bar{n} + 1)[(1 + \cosh 4\phi_j)/2]^{1/2}$ is larger than this product for an undriven mode. This indicates that, overall, *the driving enhances fluctuations*.

The response of a driven mode to a weak probe force $F_p \cos(\omega_p t)$ can be described by the linear response theory [35, 42]. We are interested in the case of resonant driving, where the frequencies of both the strong drive and the weak probe are close to the oscillator eigenfrequency, $|\omega_p - \omega_0|, |\omega_d - \omega_0| \ll \omega_0$. For the oscillator localized near a j th stable state, the resonant increment in the oscillator displacement, which is linear in the probe field, has the form

$$\langle \delta q_j(t) \rangle = \frac{1}{2} F_p \left[\chi_j(\omega_p) e^{-i\omega_p t} + \mathcal{X}_j(\omega_p) e^{i(2\omega_d - \omega_p)t} \right] + \text{c.c.} \quad (7)$$

[generally, there is also a characteristic term that comes from the probe-field induced change of the rates of fluctuation-induced switching between the states $j = 1, 2$ [35, 42]; in micromechanical systems the effect of this

term was studied by Stambaugh and Chan [51]].

The susceptibility $\chi_j(\omega_p)$ describes the response at the probe frequency ω_p . In contrast, the susceptibility \mathcal{X}_j shows the occurrence of the probe-induced vibrations at the combination frequency $2\omega_d - \omega_p$. Formally, it describes a resonant 3-photon process, in the language of nonlinear optics, which involves two photons of the strong field and one photon of the probe. Also formally, the higher-order terms that involve more than two photons of the strong field seem to have been disregarded. However, in reality both susceptibilities χ_j and \mathcal{X}_j are multiphoton: the strong field “prepares” the stable state j as a result of a process in which there participate many photons of the strong field.

A. Resonant peaks of the susceptibilities

A clear manifestation of the multiphoton nature of the susceptibilities is that they display sharp resonant peaks at the probe field frequencies $\omega_p \approx \omega_d \pm \omega_j$. Using the results [42] and Eq. (5) and assuming that

$$|\omega_p - \omega_d - \mathcal{S}\omega_j| \ll \omega_j, \quad \mathcal{S} = \pm 1,$$

one can write the resonant susceptibilities in the form:

$$\begin{aligned} \chi_j(\omega_p) &\approx \frac{i}{4\omega_d} \frac{1 + (-1)^{j-1} \mathcal{S} \cosh 2\phi_j}{\Gamma - i(\omega_p - \omega_d - \mathcal{S}\omega_j)}, \\ \mathcal{X}_j(\omega_p) &= \frac{-i}{4\omega_d} \frac{(-1)^{j-1} \mathcal{S} \sinh 2\phi_j}{\Gamma - i(\omega_p - \omega_d - \mathcal{S}\omega_j)}. \end{aligned} \quad (8)$$

Equation (8) expresses both susceptibilities in terms of the squeezing parameter ϕ_j . It suggests a way of measuring this parameter by measuring the susceptibilities.

The parameters $|\chi_j|^2$ and $|\mathcal{X}_j|^2$ give the squares of the amplitudes of the probe-field induced vibrations at frequencies ω_p and $2\omega_d - \omega_p$. The dependence of the squared amplitudes on ω_p is described by the Lorentzian peaks centered at $\omega_p = \omega_d \pm \omega_j$, with halfwidth Γ . For $\chi_j(\omega)$, the areas of the peaks

$$\mathcal{A}_j^\pm = \int_{|\omega_p - \omega_d \mp \omega_j| \ll \omega_j} |\chi_j(\omega_p)|^2 d\omega_p$$

are

$$\mathcal{A}_j^{(\pm)} = \frac{\pi}{16\omega_d^2} [1 \pm (-1)^{j-1} \cosh 2\phi_j]^2. \quad (9)$$

The ratio $\mathcal{A}_j^+/\mathcal{A}_j^- = (\tanh \phi_1)^{-4}$ for $j = 1$ and $(\tanh \phi_2)^4$ for $j = 2$, which makes it possible immediately extract the parameter ϕ_j from the experiment.

It is instructive to compare the result (8) with the susceptibility of the mode in the absence of strong driving. In the weak-noise limit, this susceptibility has the form $\chi(\omega_p) = (i/2\omega_0)[\Gamma - i(\omega_p - \omega_0)]^{-1}$. This expression coincides with Eq. (8) for $\chi_1(\omega_p)$ if in the latter expression we set $j = \mathcal{S} = 1$ (there is only one vibrational branch), $\omega_d = \omega_0$, and $\phi_1 = 0$.

The imaginary part of the susceptibility $\text{Im } \chi_j(\omega_p)$ describes the absorption of the probe field by the mode. In equilibrium it is always positive. However, as seen from Eq. (8) $\text{Im } \chi_j(\omega_p)$, has a negative Lorentzian peak at frequency $\omega_p = \omega_d + \mathcal{S}\omega_j$ for $(-1)^{j-1}\mathcal{S} < 0$. In other words, for a given branch of the forced vibrations j , one of the peaks of $\text{Im } \chi_j(\omega_p)$ is positive and the other is negative. The negative sign of $\text{Im } \chi_j(\omega_p)$ indicates that the mode is amplifying the probe signal rather than absorbing energy from it. The amplification comes at the expense of the strong drive. However, overall $\int d\omega_p \text{Im } \chi_j(\omega_p) = \pi/2\omega_d$ is positive, a well-known feature of an oscillator [52].

The ratio of the areas of the peaks of $|\text{Im } \chi_j(\omega_p)|$ at $\omega_p = \omega_d \pm \omega_j$ is

$$\begin{aligned} Q_1^+ / Q_1^- &= \tanh^{-2} \phi_1, & Q_2^+ / Q_2^- &= \tanh^2 \phi_2, \\ Q_j^\pm &= \int_{|\omega_p - \omega_d \mp \omega_j| \ll \omega_j} |\text{Im } \chi_j(\omega_p)| d\omega_p \end{aligned} \quad (10)$$

It should be noted that, in the quantum domain, the theory applies for sufficiently large vibration amplitude where, beside the condition $\omega_j \gg \Gamma$, there also holds the condition that many quantum levels of the mode are occupied, $\omega_d A_j^2 / \hbar \gg 1$. The other quantum restriction on the applicability of Eq. (8) is that the nonequidistance of the quasienergy levels (Floquet eigenvalues) of the driven mode, which is a consequence of the nonlinearity, is small compared the dissipative level broadening. To the order of magnitude, it corresponds to $\hbar|\gamma| < \Gamma\omega_d^2(2\bar{n} + 1)$; a more exact condition is given in Ref. [2]. Even where this condition does not hold, the expressions for the areas of the spectral peaks (9) still apply.

B. Exact tuning of the strong driving force

The above expressions simplify in the case where the frequency of the strong driving force ω_d is equal to the mode eigenfrequency ω_0 . In this case there is only one branch of forced vibrations, $j = 1$. As seen from Eq. (5),

$$\phi \equiv \phi_1 = (\ln 3)/4 \quad (\omega_d = \omega_0). \quad (11)$$

The squeezing parameter (11) is independent of the force amplitude F_d . The corresponding value of $\exp(4\phi) = 3$ is shown by the dashed lines in Fig. 3. It was this case that we studied in the experiment to demonstrate the efficiency of the method. For the studied classical mode, $k_B T \gg \hbar\omega_d$, we have from Eq. (4)

$$\begin{aligned} \langle \delta Q^2 \rangle &\equiv \langle \delta Q_1^2 \rangle \approx 2k_B T / 3\omega_d^2, \\ \langle \delta P^2 \rangle &\equiv \langle \delta P_1^2 \rangle \approx 2k_B T / \omega_d^2. \end{aligned} \quad (12)$$

We use these expressions in discussing the data.

V. RESULTS

In order to compare the theoretical model with the experimental data, we add the expected position of the

two satellites according to Eq. (3) as a red dotted line in Fig. 2(a). We find excellent agreement between the model (with no free parameters) and the experiment. To further analyze our data, we focus on the imaginary part of the susceptibility. It determines the quadrature component which is directly determined from the response measurement (see black trace in Fig. 2(b)).

Clearly, the different signs of the satellite peaks predicted by the model and attributed to the absorption and amplification of the probe field are recovered. The absorption is observed for the higher frequency satellite with the higher intensity, whereas the amplification is visible in the weaker and lower frequency satellite. We do not measure the power of the probe field at the output, but the very fact that the resonantly absorbed power $(\omega_p F_p^2/2)\text{Im } \chi_j(\omega_p)$ is negative for $\text{Im } \chi_j(\omega_p) < 0$ unambiguously indicates that the nanostring pumps energy into the probe field.

According to Eq. (8) the satellites in the imaginary part of the susceptibility $|\text{Im } \chi_1(\omega_p)|$ have a Lorentzian lineshape. Thus, Lorentzian fits are employed to extract the area enclosed under the satellites, Q_1^+ and Q_1^- . The area ratio Q_1^+ / Q_1^- extracted from the imaginary part of the susceptibility is plotted in Fig. 4(a) as black dots and compared with the theoretical model according to Eq. (10) included as a red line. No free parameters are employed. We find excellent agreement between the experiment and the theory. We note that the amplitude of the signal, i.e. the blue dotted line in Fig. 2(b), which is given by $|\chi_j(\omega_p)| \propto [\Gamma^2 + (\omega_p - \omega_d)^2]^{-1/2}$ is a non-Lorentzian function of ω_p . It falls off slower than the Lorentzian with the increasing $|\omega_p - \omega_d|$, as indeed seen in Fig. 2(b).

It is expected from Eq. (12) that the squeezing parameter is independent of the drive amplitude F_d if the drive frequency coincides with the eigenfrequency of the mode. Such independence is indeed seen in the experiment, which yields an average squeezing parameter of 0.2825 ± 0.0295 in good agreement with the theoretically obtained value of 0.2747. This confirms not only the analysis of the squeezing, but also the model we use to describe the mode dynamics.

In Fig. 4(b), the result is re-expressed in terms of the mean-square fluctuations of the in-phase and quadrature component $\langle \delta Q^2 \rangle$ and $\langle \delta P^2 \rangle$, Eq. (4). The experimental data is plotted as black and gray dots, respectively, whereas the theoretical predictions obtained using Eq. (12) are shown as red lines. For the sake of clarity, we chose a normalized dimensionless representation. This obviates reintroducing the effective mass of the resonator, which would otherwise re-appear in the denominator of Eqs. (4) and (12). The grey dashed line indicates the mean-square of the thermomechanical fluctuations at 293 K, clearly showing that a significant squeezing of the in-phase component is observed.

We note that the data spread in Fig. 4(a) and (b) is larger for weak drive power as a result of an insufficient separation of the satellite peaks. There is also a small

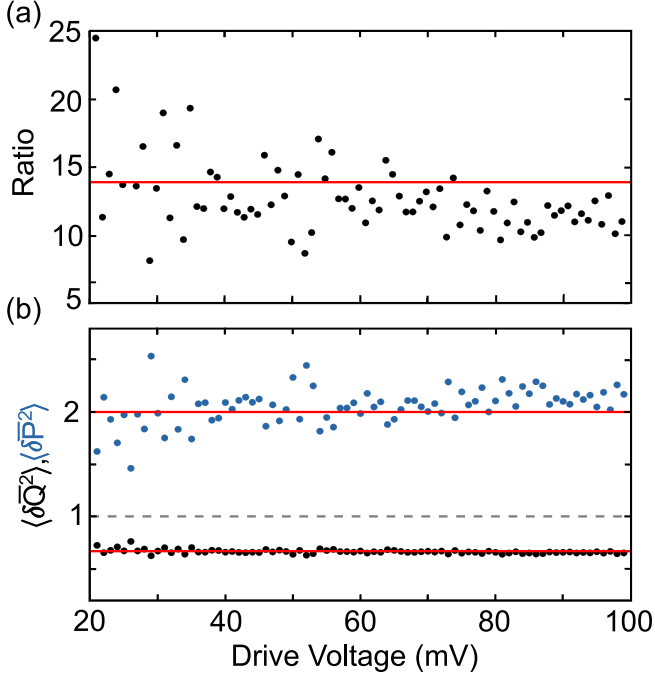


Figure 4. (a) Ratio of the areas of the satellites peaks obtained from the quadrature data as a function of the drive voltage (black dots). Red line corresponds to the theoretical prediction. (b) Normalized dimensionless variances of the in-phase and quadrature fluctuations $\langle \delta \bar{Q}^2 \rangle = (\omega_0^2/k_B T) \langle \delta Q^2 \rangle$ and $\langle \delta \bar{P}^2 \rangle = (\omega_0^2/k_B T) \langle \delta P^2 \rangle$ around the stable state of the forced vibration as functions of the drive voltage. Black and blue dots show the in-phase and quadrature values extracted from the experimentally determined satellite area ratio from panel (a), whereas the red lines show the corresponding theoretical model of Eq. (12). Grey dashed line illustrates the thermomechanical fluctuations at the temperature 293 K used in the experiment.

systematic tilt arising from a deviation from the Duffing model that comes into play for large drive powers.

VI. CONCLUSION

This paper presents the spectra of the response of a moderately strongly driven nanomechanical mode to a weak probe drive. The frequencies of the strong drive and the probe tone are close to the mode eigenfrequency. We found that the response spectra of our very weakly damped mode have a peculiar structure. Both the amplitude of the response and the quadrature component display two pronounced features symmetrically located with respect to the strong-drive frequency. The features on the high-frequency side are more pronounced than on the low-frequency side. In the case of the amplitude, the features are non-Lorentzian peaks. In contrast, the quadrature component displays a peak on the high-frequency side and a dip on the low-frequency side. Both have a Lorentzian shape with the same halfwidth as the

peak in the spectrum of the mode in the absence of strong driving.

The theory predicts the onset of these features. The distance along the frequency axis between the features and the frequency of the strong drive is expected to be equal to the frequency of oscillations of the strongly driven nonlinear mode about its stable state of forced vibrations. This frequency, in turn, is determined by the interplay of the strong drive and the mode nonlinearity. Therefore, in terms of quantum optics, the occurrence of the features of the response is a result of multiphoton processes that involve multiple quanta of the strong drive.

The amplitude and the quadrature component of the probe-induced vibrations are determined, respectively, by the absolute value and the imaginary part of the susceptibility of the mode with respect to the probe. The dip in the quadrature spectrum corresponds to a negative imaginary part of the susceptibility. This indicates that the weak probe drive is amplified by the mode. The amplification comes at the expense of the energy provided by the strong drive.

The strongly driven mode is a system away from thermal equilibrium. Therefore there is no standard relation between the imaginary part of the susceptibility and the spectrum of fluctuations of the mode. Nevertheless it is clear on the physical grounds that there should be some relations between these spectra for the considered weakly damped mode. Indeed, in the rotating frame, the stable state of forced vibrations is a stationary state. The weakly damped mode oscillates about this state due to thermal and quantum noise, but these oscillations can be also resonantly excited by an external drive. Therefore the power spectrum and the susceptibility should display features at the same frequencies. The susceptibility thus encodes some information about the fluctuations.

The theoretical analysis shows that one of the components of the fluctuations should be squeezed and that the squeezing determines the ratio of the areas of the dip and the peak in the imaginary part of the susceptibility. Therefore by measuring these areas one can extract the squeezing parameter. Moreover, the theory predicts that, if the frequency of the strong drive is equal to the mode eigenfrequency, the ratio of the areas should be independent of the drive amplitude and should be equal to $7 + 4\sqrt{3} \approx 13.9$. This is in excellent agreement with the experiment. Our findings have been independently reproduced on a second sample.

The agreement between the experiment and the theory regarding the measured positions of the peaks of the susceptibility, their shape, and their areas, with no adjustable parameters, provides a strong evidence of the squeezing of fluctuations expected in the theoretical analysis. It complements and significantly extends the results on the shape and the area of the classical power spectra of a driven mode [40]. The extension is particularly important as the method presented in Ref. [40] is applicable only in the classical regime, whereas both classical and

quantum fluctuations are squeezed. The present method, although the experiment is done in the classical regime, does not rely on and does not require that the fluctuations be classical. To the best of our knowledge, the results also present the first observation of a multiphoton resonant amplification by a driven nonlinear vibrational mode. They demonstrate new interdisciplinary aspects of the studies of nanomechanical systems.

VII. ACKNOWLEDGEMENTS

J. S. O. and E. M. W. gratefully acknowledge financial support by the Deutsche Forschungsgemeinschaft via

the collaborative research center SFB 767, the European Unions Horizon 2020 Research and Innovation Programme under Grant Agreement No 732894 (FET Proactive HOT), and the German Federal Ministry of Education and Research (contract no. 13N14777) within the European QuantERA cofund project QuaSeRT. M. I. D. acknowledges support from the National Science Foundation, Grants No. DMR-1806473 and CMMI 1661618. M. I. D. is a senior fellow of the Zukunftskolleg of the University of Konstanz; he is grateful for the warm hospitality at the University of Konstanz where this work was started. The authors thank Gianluca Rastelli and Wolfgang Belzig for fruitful discussions and comments about this work. Data and analysis code are available at XXX.

-
- [1] A. N. Cleland, *Foundations of Nanomechanics: From Solid-State Theory to Device Applications* (Springer, Berlin, 2003).
- [2] M. I. Dykman, ed., *Fluctuating Nonlinear Oscillators: From Nanomechanics to Quantum Superconducting Circuits* (Oxford University Press, Oxford, 2012).
- [3] S. Schmid, L. G. Villanueva, and M. L. Roukes, *Fundamentals of Nanomechanical Resonators* (Springer, Switzerland, 2016).
- [4] A. D. O'Connell, M. Hofheinz, M. Ansmann, R. C. Bialczak, M. Lenander, E. Lucero, M. Neeley, D. Sank, H. Wang, M. Weides, J. Wenner, J. M. Martinis, and A. N. Cleland, Quantum Ground State and Single-Phonon Control of a Mechanical Resonator, *Nature* **464**, 697 (2010).
- [5] K. J. Satzinger, Y. P. Zhong, H.-S. Chang, G. A. Peairs, A. Bienfait, M.-H. Chou, A. Y. Cleland, C. R. Conner, E. Dumur, J. Grebel, I. Gutierrez, B. H. November, R. G. Povey, S. J. Whiteley, D. D. Awschalom, D. I. Schuster, and A. N. Cleland, Quantum Control of Surface Acoustic-Wave Phonons, *Nature* **563**, 661 (2018).
- [6] Y. Chu, P. Kharel, T. Yoon, L. Frunzio, P. T. Rakich, and R. J. Schoelkopf, Creation and Control of Multi-Phonon Fock States in a Bulk Acoustic-Wave Resonator, *Nature* **563**, 666 (2018).
- [7] Y. Tsaturyan, A. Barg, E. S. Polzik, and A. Schliesser, Ultracoherent Nanomechanical Resonators via Soft Clamping and Dissipation Dilution, *Nat Nanotech* **12**, 776 (2017).
- [8] A. H. Ghadimi, S. A. Fedorov, N. J. Engelsen, M. J. Breyhi, R. Schilling, D. J. Wilson, and T. J. Kippenberg, Elastic Strain Engineering for Ultra-Low Mechanical Dissipation, *Science* **360**, 764 (2018).
- [9] E. Buks and M. L. Roukes, Metastability and the Casimir Effect in Micromechanical Systems, *Eur. Lett* **54**, 220 (2001).
- [10] H. W. C. Postma, I. Kozinsky, A. Husain, and M. L. Roukes, Dynamic Range of Nanotube- and Nanowire-Based Electromechanical Systems, *Appl Phys Lett* **86**, 223105 (2005).
- [11] J. S. Aldridge and A. N. Cleland, Noise-Enabled Precision Measurements of a Duffing Nanomechanical Resonator, *Phys Rev Lett* **94**, 156403 (2005).
- [12] C. Stambaugh and H. B. Chan, Noise Activated Switching in a Driven, Nonlinear Micromechanical Oscillator, *Phys Rev B* **73**, 172302 (2006).
- [13] N. Kacem and S. Hentz, Bifurcation Topology Tuning of a Mixed Behavior in Nonlinear Micromechanical Resonators, *APL* **95**, 183104 (2009).
- [14] Q. P. Unterreithmeier, T. Faust, and J. P. Kotthaus, Nonlinear Switching Dynamics in a Nanomechanical Resonator, *Phys Rev B* **81**, 241405 (2010).
- [15] M. Defoort, V. Puller, O. Bourgeois, F. Pistoletti, and E. Collin, Scaling Laws for the Bifurcation Escape Rate in a Nanomechanical Resonator, *Phys Rev E* **92**, 050903 (2015).
- [16] R. J. Dolleman, P. Belardinelli, S. Houri, H. S. J. van der Zant, F. Alijani, and P. G. Steeneken, High-Frequency Stochastic Switching of Graphene Resonators Near Room Temperature, *Nano Lett* **19**, 1282 (2019).
- [17] A. Erbe, H. Krömmmer, A. Kraus, R. H. Blick, G. Corso, and K. Richter, Mechanical mixing in nonlinear nanomechanical resonators, *Appl. Phys. Lett.* **77**, 3102 (2000).
- [18] R. B. Karabalin, M. C. Cross, and M. L. Roukes, Nonlinear Dynamics and Chaos in Two Coupled Nanomechanical Resonators, *Phys Rev B* **79**, 165309 (2009).
- [19] H. J. R. Westra, M. Poot, H. S. J. van der Zant, and W. J. Venstra, Nonlinear Modal Interactions in Clamped-Clamped Mechanical Resonators, *Phys Rev Lett* **105**, 117205 (2010).
- [20] A. Eichler, M. del Álamo Ruiz, J. A. Plaza, and A. Bachtold, Strong Coupling between Mechanical Modes in a Nanotube Resonator, *Phys Rev Lett* **109**, 025503 (2012).
- [21] A. Castellanos-Gómez, H. B. Meerwaldt, W. J. Venstra, H. S. J. van der Zant, and G. A. Steele, Strong and Tunable Mode Coupling in Carbon Nanotube Resonators, *Phys Rev B* **86**, 041402 (2012).
- [22] I. Mahboob, N. Perrin, K. Nishiguchi, D. Hatanaka, Y. Okazaki, A. Fujiwara, and H. Yamaguchi, Dispersive and Dissipative Coupling in a Micromechanical Resonator Embedded with a Nanomechanical Resonator, *Nano Lett* **15**, 2312 (2015).
- [23] J. Güttinger, A. Noury, P. Weber, A. M. Eriksson, C. Lagoin, J. Moser, C. Eichler, A. Wallraff, A. Isacsson, and A. Bachtold, Energy-Dependent Path of Dissipation in Nanomechanical Resonators, *Nat Nano* **12**, 631 (2017).

- [24] M. J. Seitner, M. Abdi, A. Ridolfo, M. J. Hartmann, and E. M. Weig, Parametric Oscillation, Frequency Mixing, and Injection Locking of Strongly Coupled Nanomechanical Resonator Modes, *Phys. Rev. Lett.* **118**, 254301 (2017).
- [25] D. A. Czaplewski, C. Chen, D. Lopez, O. Shoshani, A. M. Eriksson, S. Strachan, and S. W. Shaw, Bifurcation Generated Mechanical Frequency Comb, *Phys Rev Lett* **121**, 244302 (2018).
- [26] M. Aspelmeyer, T. Kippenberg, and F. Marquardt, eds., *Cavity Optomechanics: Nano- and Micromechanical Resonators Interacting with Light* (Springer, Berlin, 2014).
- [27] C. M. Caves, Quantum-Mechanical Noise in an Interferometer, *Phys Rev D* **23**, 1693 (1981).
- [28] M. Tse *et al.*, Quantum-Enhanced Advanced LIGO Detectors in the Era of Gravitational-Wave Astronomy, *Phys. Rev. Lett.* **123**, 231107 (2019).
- [29] F. Acernese *et al.*, Increasing the Astrophysical Reach of the Advanced Virgo Detector via the Application of Squeezed Vacuum States of Light, *Phys. Rev. Lett.* **123**, 231108 (2019).
- [30] E. E. Wollman, C. U. Lei, A. J. Weinstein, J. Suh, A. Kronwald, F. Marquardt, A. A. Clerk, and K. C. Schwab, Quantum squeezing of motion in a mechanical resonator, *Science* **349**, 952 (2015).
- [31] F. Lecocq, J. B. Clark, R. W. Simmonds, J. Aumentado, and J. D. Teufel, Quantum Nondemolition Measurement of a Nonclassical State of a Massive Object, *Phys. Rev. X* **5**, 041037 (2015).
- [32] J.-M. Pirkkalainen, E. Damskägg, M. Brandt, F. Massel, and M. A. Sillanpää, Squeezing of Quantum Noise of Motion in a Micromechanical Resonator, *Phys Rev Lett* **115**, 243601 (2015).
- [33] D. Rugar and P. Grütter, Mechanical Parametric Amplification and Thermomechanical Noise Squeezing, *Phys Rev Lett* **67**, 699 (1991).
- [34] D. F. Walls and G. J. Milburn, *Quantum Optics* (Springer, Berlin, 2008).
- [35] M. I. Dykman and M. A. Krivoglaz, Theory of Fluctuational Transitions between the Stable States of a Non-Linear Oscillator, *Zh Eksp Teor Fiz* **77**, 60 (1979).
- [36] A. P. Dmitriev and M. I. Dyakonov, Activation and Tunnel Transitions between 2 Forced Oscillation Regimes of an Anharmonic-Oscillator, *Zh Eksp Teor Fiz* **90**, 1430 (1986).
- [37] E. Buks and B. Yurke, Mass Detection with a Nonlinear Nanomechanical Resonator, *Phys Rev E* **74**, 046619 (2006).
- [38] R. Almog, S. Zaitsev, O. Shtempluck, and E. Buks, Noise Squeezing in a Nanomechanical Duffing Resonator, *Phys Rev Lett* **98**, 078103 (2007).
- [39] K. Y. Fong, W. H. P. Pernice, and H. X. Tang, Frequency and Phase Noise of Ultrahigh Q Silicon Nitride Nanomechanical Resonators, *Phys Rev B* **85**, 161410 (R) (2012).
- [40] J. S. Huber, G. Rastelli, M. J. Seitner, J. Kölbl, W. Belzig, M. I. Dykman, and E. M. Weig, Spectral Evidence of Squeezing of a Weakly Damped Driven Nanomechanical Mode, *Phys. Rev. X* **10**, 021066 (2020).
- [41] M. I. Dykman, Periodically Modulated Quantum Nonlinear Oscillators, in *Fluctuating Nonlinear Oscillators: From Nanomechanics to Quantum Superconducting Circuits*, edited by M. I. Dykman (Oxford University Press, Oxford, 2012) pp. 165–197.
- [42] M. I. Dykman, D. G. Luchinsky, R. Mannella, P. V. E. McClintock, N. D. Stein, and N. G. Stocks, Supernarrow Spectral Peaks and High-Frequency Stochastic Resonance in Systems with Coexisting Periodic Attractors, *Phys Rev E* **49**, 1198 (1994).
- [43] T. Antoni, K. Makles, R. Braive, T. Briant, P.-F. Chodron, I. Sagnes, I. Robert-Philip, and A. Heidmann, Nonlinear mechanics with suspended nanomembranes, *EPL* **100**, 68005 (2012).
- [44] Y. R. Shen, *The Principles of Nonlinear Optics*, 1st ed. (Wiley, New York, 1984).
- [45] Q. P. Unterreithmeier, E. M. Weig, and J. P. Kotthaus, Universal transduction scheme for nanomechanical systems based on dielectric forces, *Nature* **458**, 1001 (2009).
- [46] T. Faust, P. Krenn, S. Manus, J. Kotthaus, and E. Weig, Microwave cavity-enhanced transduction for plug and play nanomechanics at room temperature, *Nature Communications* **3**, (2012).
- [47] J. Rieger, T. Faust, M. J. Seitner, J. P. Kotthaus, and E. M. Weig, Frequency and q factor control of nanomechanical resonators, *Applied Physics Letters* **101**, 103110 (2012).
- [48] T. Faust, J. Rieger, M. J. Seitner, J. P. Kotthaus, and E. M. Weig, Coherent control of a classical nanomechanical two-level system, *Nature Physics* **9**, 485 (2013).
- [49] L. D. Landau and E. M. Lifshitz, *Electrodynamics of Continuous Media*, 2nd ed. (Elsevier Butterworth-Heinemann, Oxford, 2004).
- [50] L. D. Landau and E. M. Lifshitz, *Mechanics*, 3rd ed. (Elsevier, Amsterdam, 2004).
- [51] C. Stambaugh and H. B. Chan, Supernarrow Spectral Peaks near a Kinetic Phase Transition in a Driven Nonlinear Micromechanical Oscillator, *Phys Rev Lett* **97**, 110602 (2006).
- [52] A. M. Perelomov and Y. B. Zel'dovich, *Quantum Mechanics: Selected Topics* (World Scientific, Singapore, 1998).